

# Why are Frictionless Packings of Ellipse-Shaped Particles Hypostatic?

Mitch Mailman<sup>1</sup>, Carl F. Schreck<sup>2</sup>, Corey S. O'Hern<sup>2</sup> and Bulbul Chakraborty<sup>1</sup>

<sup>1</sup>Martin Fisher School of Physics, Brandeis University, Mail Stop 057, Waltham, MA 02454-9110, USA

<sup>2</sup>Department of Mechanical Engineering, Yale University, New Haven, CT

06520-8284 and Department of Physics, Yale University, New Haven CT 06520-8120

(Dated: May 29, 2019)

We study the structural and mechanical properties of static packings of frictionless ellipses that interact via a pairwise, repulsive harmonic interparticle potential that penalizes ellipse overlap. Over a range of aspect ratios, the static packings are hypostatic with more degrees of freedom than constraints. We analyze the mechanical stability of these hypostatic packings, and find that the vibrational spectrum differs significantly from that of disk packings, possessing three distinct branches. In the limit of zero compression, the energy of the modes in the lowest branch increases *quartically* with the deformation amplitude, and the density of states possesses a  $\delta$ -function at zero frequency. We identify scaling relations that collapse the low-frequency part of the vibrational spectra for different aspect ratios. Finally, we find that the degree of hypostaticity is determined by the number of quartic modes.

PACS numbers: 61.43.-j, 81.05.Kf, 63.50.Lm, 83.80.Fg

About a decade ago, Liu and Nagel proposed that jamming transitions in glassy, granular, and other amorphous systems can be described by the jamming phase diagram [1], and that a ‘fixed point’ (Point J) in the jamming phase diagram controls slow dynamics in these systems even far from Point J [2]. For disordered systems composed of frictionless, spherical grains interacting via purely repulsive, short-range potentials, the packings at Point J are *isostatic* [3, 4], where the number of degrees of freedom exactly matches the number of constraints. Isostatic particle packings show interesting mechanical properties; for example, they are characterized by an abundance of spatially extended “floppy modes” of excitation [5, 6, 7]. In this letter, we focus instead on static packings of *anisotropic*, frictionless particles near Point J, and determine their structural and mechanical properties.

For a static packing of  $N$  grains in  $d$  spatial dimensions, with  $d - 1$  rotational and  $d$  translational degrees of freedom per grain, total force and torque balance on each grain can be satisfied only if the total number of contacts satisfies  $N_c \geq N_f \equiv N(2d - 1)$  in the large system limit. Isostatic packings satisfy  $N_c = N_f$ , while hypostatic packings possess  $N_c < N_f$ . In contrast to spherical particle packings, static packings of ellipsoidal particles, studied previously by Donev, *et al.* [8], are generically hypostatic and possess higher densities without translational and orientational order. Experiments on packings of ellipsoidal M&M candies have also verified these results[9]. These previous studies raise several fundamental questions about static packings of ellipsoidal particles; for example, why are they hypostatic and what is the nature of their low-energy excitations? In this letter, we study the low-energy, vibrational excitations of 2D static packings of ellipses using a numerical packing-generation algorithm in which soft ellipses interact via purely repulsive potentials at zero temperature. Our analysis demonstrates the existence of two gaps in the vibrational spectrum over a range of aspect ratios. The energy of the modes below the first gap increases *quartically* with deformation amplitude along the soft direc-

tions, and the number of these quartic modes determines the degree of hypostaticity of the packings.

*Compression packing-generation protocol* We generated an extensive set of static packings of ellipses over a range of system sizes from  $N = 120$  to 1920, in which particles are ‘just touching’, using a numerical packing-generation protocol similar to that employed to create static packings of spherical particles [10, 11]. We will refer to this protocol as the ‘compression method’. In this method, soft, purely repulsive ellipses are first randomly deposited in a square cell with periodic boundary conditions at a low packing fraction ( $\phi = 0.5$ ). The configurations are successively compressed in small steps ( $\Delta\phi = 10^{-4}$ ) and then relaxed using conjugate energy minimization after each step. Near the jamming packing fraction  $\phi_J$ , where the particles are just touching, the configurations are expanded or compressed by decreasing amounts until the system has vanishingly small total potential energy per particle  $V_{\text{tol}} < V < 2V_{\text{tol}}$ .  $V_{\text{tol}} = 10^{-12}$  for most simulations,  $V = \sum_{i>j} V(r_{ij})$  summed over all ellipse pairs,

$$V(r_{ij}) = \begin{cases} (1 - r_{ij}/\sigma_{ij})^2 & r_{ij} \leq \sigma_{ij} \\ 0 & r_{ij} > \sigma_{ij}, \end{cases} \quad (1)$$

and  $r_{ij}$  is the separation between the centers of mass of ellipses  $i$  and  $j$ . The separations and orientations  $\hat{u}_i$  and  $\hat{u}_j$  of the long axes of ellipses  $i$  and  $j$  determine the Perram and Wertheim overlap parameter [12, 13, 14, 15]

$$\sigma_{ij} = \min_{\lambda} \frac{\sigma_0(\lambda)}{\sqrt{1 - \frac{\chi(\lambda)}{2} \sum_{\pm} \frac{\beta(\lambda) \hat{r}_{ij} \cdot \hat{u}_i \pm \beta^{-1}(\lambda) \hat{r}_{ij} \cdot \hat{u}_j}{1 \pm \chi(\lambda) \hat{u}_i \cdot \hat{u}_j}}}, \quad (2)$$

where  $\sigma_0$ ,  $\beta$ , and  $\chi$  depend on  $\lambda$  and the major (minor) axis,  $a_i$  ( $b_i$ ), of the  $i$ th ellipse [16]. To determine  $\sigma_{ij}$  for each pair, minimization of the parameter  $0 < \lambda < 1$  must be performed. We simulate bidisperse mixtures to inhibit translational and orientational order: one-third of the particles are large with

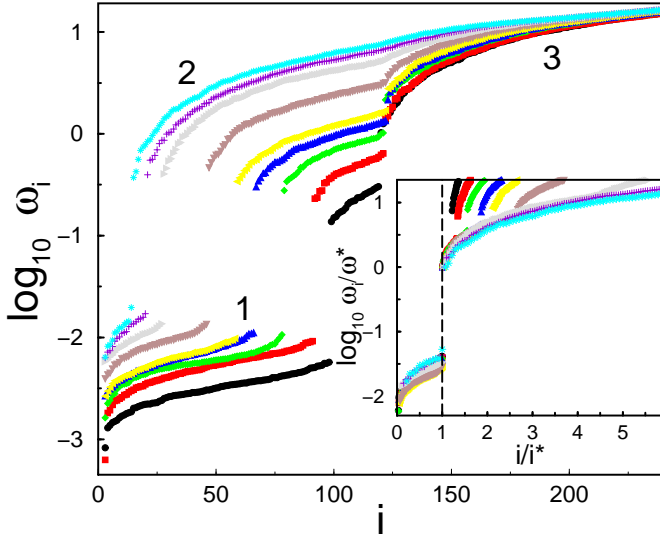


FIG. 1: (Color online) Normal mode frequencies  $\omega_i$  obtained from the dynamical matrix (Eq. 3) vs. index  $i$ , sorted by increasing frequency for  $N = 120$  static ellipse packings at nine aspect ratios,  $\alpha = 1.02$  (black), 1.04 (red), 1.06 (green), 1.08 (blue), 1.1 (yellow), 1.2 (brown), 1.4 (gray), 1.6 (violet), and 1.80 (turquoise). The sorted frequency spectrum possesses three distinct branches (numbered 1, 2, and 3) as discussed in the text. In the inset, we show the scaled frequency  $\omega_i/\omega^*$  vs.  $i/i^*$ , which collapses the low frequency part of the spectra at 1 (vertical dashed line).

the major axis 1.4 times that of the small particles [8]. Using this procedure, we generated an ensemble of at least 100 ellipse packings, each characterized by the jamming packing fraction  $\phi_j$ , over a range of aspect ratios from  $\alpha = 1$  to 2. We calculated the global bond-orientational and nematic order parameters for the ellipse packings [17] and found no significant ordering with order parameters  $\sim 1/\sqrt{N}$  for all  $\alpha$ .

*Vibrational Spectra* To determine the mechanical properties of the static ellipse packings, we calculate the dynamical matrix defined as

$$M_{mn} = \frac{\partial^2 V}{\partial \xi_m \partial \xi_n}, \quad (3)$$

where  $\xi_m = \{x_m, y_m, a_m \theta_m\}$ ,  $a_m$ ,  $x_m$  and  $y_m$  are the major axis and center of mass coordinates of ellipse  $m$ ,  $\theta_m$  is the angle between  $\hat{u}_m$  and the  $x$ -axis, and  $m, n = 1, \dots, N$  [18]. When Eq. 3 is evaluated for a static ellipse packing and diagonalized using periodic boundary conditions, in principle one obtains  $(2d-1)N' - d$  nontrivial vibrational eigenmodes, where  $N' = N - N_r$  and  $N_r$  is the number of ‘rattlers’ with fewer than  $d+1$  contacts. If we assume that all ellipses have the same mass, the square roots of the eigenvalues of the dynamical matrix give the normal mode frequencies  $\omega_i$  indexed by  $i$ . We denote the normalized eigenvector corresponding to  $\omega_i$  by  $\hat{e}_i = \{e_{xi}^{j=1}, e_{yi}^{j=1}, e_{\theta i}^{j=1}, \dots, e_{xi}^{j=N'}, e_{yi}^{j=N'}, e_{\theta i}^{j=N'}\}$  with the constraint that  $\hat{e}_i^2 = 1$ . Below, we will show the relative contributions of translational and orientational components of the eigenvectors, for example, the translational contribution from mode  $i$  is  $T_i = \sum_{j=1}^{N'} \{(e_{xi}^j)^2 + (e_{yi}^j)^2\}$  and  $R_i = 1 - T_i$ .

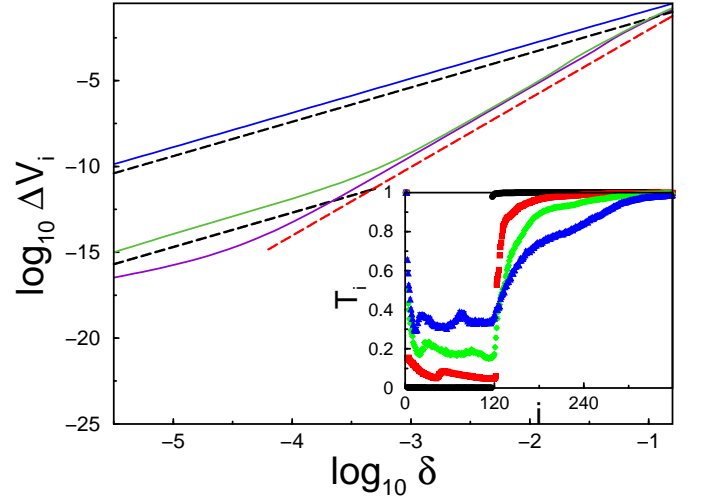


FIG. 2: (Color online) Change in potential energy  $\Delta V_i$  vs. displacement  $\delta$  along  $\hat{e}_i$  for  $N = 120$  and  $\alpha = 1.5$  ( $i^* = 22$ ).  $\Delta V_i$  (solid blue) for  $i = 115 > i^*$  is quadratic in  $\delta$ . In contrast, for  $i \leq i^*$ ,  $\Delta V_i \propto \delta^2$  for  $\delta < \delta_c$ , but  $\propto \delta^4$  for  $\delta > \delta_c$ . For  $i = 24$ , we show that  $\delta_c$  decreases from approximately  $10^{-3}$  to  $10^{-4}$  as  $V_{\text{tot}}$  varies from  $10^{-12}$  (green) to  $10^{-16}$  (purple). The dashed black and red lines have slope two and four, respectively. Inset: The translational contribution  $T_i$  to the sum of the squares of the amplitudes of each eigenvector  $\hat{e}_i$  of the dynamical matrix for aspect ratio  $\alpha = 1.01$  (black), 1.20 (red), 1.50 (green), and 2.00 (blue).

Over a range of aspect ratios, the spectrum  $\omega_i$ , sorted in order of increasing frequency, possesses three distinct regimes (*cf* Fig. 1): (1) modes with indexes  $(i-2) < i^*(\alpha)$  below the low-frequency gap, (2) modes with index  $i^* \leq (i-2) \leq i_t = (d-1)N$ , where for  $\alpha \leq \alpha_t$ , there is a second gap at index  $i_t$ , and (3) modes with index  $(i-2) > i_t$ . (We are explicitly not including the two trivial modes corresponding to translational invariance.) The aspect ratio  $\alpha_t$  at which the second gap closes is approximately 1.2 for  $N = 120$  as shown in Fig. 1. In the inset to Fig. 1, we show that we are able to choose aspect ratio dependent scaling factors  $\omega^*$  and  $i^*$  that collapse the low-frequency part of the spectra including the first gap. We find that  $\omega^*$  is roughly linear with  $\alpha - 1$ , while  $i^*$  possesses two different scaling regimes for  $\alpha - 1 \ll 1$  and  $\alpha > 1$  that will be discussed in detail below. As demonstrated in the inset to Fig. 2, modes in regions (1) and (2) are mainly rotational in character, whereas those in region (3) correspond to mainly translational motion.

We find that our static ellipse packings at finite, but very small overcompression possess  $(2d-1)N - d$  nonzero, positive eigenvalues [19]. To rationalize this result with the fact that hard ellipse packings are generically hypostatic [8], we perturbed our ellipse packings along each of the eigendirections of the dynamical matrix over a range of overcompression. If  $\vec{\xi}_0$  characterizes the centers of mass and orientations of the original static ellipse packing, the perturbed configuration obtained after a shift by  $\delta$  along eigenmode  $i$  and relaxation to the nearest local energy minimum is  $\vec{\xi}_i = \vec{\xi}_0 + \delta \hat{e}_i$ . In Fig. 2, we plot the change in potential energy,  $\Delta V_i \equiv V(\vec{\xi}_i) - V(\vec{\xi}_0)$ , of static ellipse packings with  $N = 120$

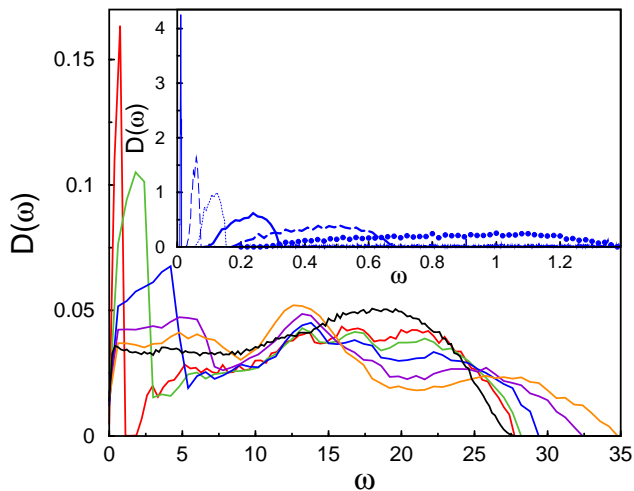


FIG. 3: Density of vibrational modes  $D(\omega)$  for static ellipse packings with  $N = 120$  over a range of aspect ratios,  $\alpha = 1.0$  (black), 1.1 (red), 1.2 (green), 1.4 (blue), 1.7 (violet), and 2.0 (orange). The low-frequency peak corresponds to rotational modes in frequency regime 2 discussed in the text. The inset magnifies the low-frequency region of  $D(\omega)$  for  $\alpha$  near 1:  $\alpha = 1.001$  (thin solid), 1.005 (thin dashed), 1.01 (thin dotted), 1.02 (thick solid), 1.04 (thick dashed), and 1.08 (filled circles). The low-frequency peak is sharp and  $D(\omega)$  possesses a gap in  $\omega$  for  $\alpha < \alpha_t \approx 1.2$ . However, the peak broadens and connects to  $D(\omega)$  at large  $\omega$  without going to zero for  $\alpha > \alpha_t$ .

at  $\alpha = 1.5$  arising from a perturbation along mode  $i$  as a function of amplitude  $\delta$  and for two values of overcompression  $V_{\text{tol}}$ . As shown in Fig. 2, for modes with indexes in regions (2) and (3) of the frequency spectrum  $\Delta V_i \propto \delta^2$  for all  $\delta$  independent of  $V_{\text{tol}}$ . In contrast, there is range  $\delta > \delta_c$  over which modes in region (1) (that number  $N_4 = i^* - 1$ ) display *quartic* dependence on  $\delta$ ,  $\Delta V_i \propto \delta^4$ , whereas  $\Delta V_i \propto \delta^2$  for  $\delta < \delta_c$ . Since  $\delta_c \sim V_{\text{tol}}^{1/4}$  for modes in region (1), quartic behavior will persist over the entire range of  $\delta$  in the zero compression limit  $V_{\text{tol}} \rightarrow 0$ . The implication of these findings is that the modes in the lowest branch of the spectrum, i.e. region (1), become true zero-frequency modes of the dynamical matrix in the limit of zero overcompression. Thus, ‘just touching’ static ellipse packings are stabilized by quartic rather than quadratic terms in the expansion of the total potential energy around the reference packing[8].

The density of vibrational modes,  $D(\omega)$ , obtained from the spectrum,  $\omega_i$ , shown in Fig. 3, exhibits several key differences from  $D(\omega)$  of bidisperse disk packings [2]. First, the plateau at small  $\omega$  characteristic of nearly-isostatic disk packings is replaced by a narrow peak at low frequencies. This peak is composed of modes in region (2) of the spectrum that display collective, primarily rotational (*not translational*) motion. For  $\alpha < \alpha_t$  (with  $\alpha_t \approx 1.2$  for  $N = 120$ ), this peak is clearly separated by a gap from the broad, high-frequency regime. Note that on a logarithmic scale one would see an additional peak that corresponds to modes in region (1), and is separated by a gap from the modes in region (2). As discussed before, this peak shifts to lower  $\omega$ , and narrows to a  $\delta$ -function at zero frequency in the zero-compression limit. Second, for large aspect ratios ( $\alpha > 1.5$  for  $N = 120$ ),  $D(\omega)$  of ellipse packings

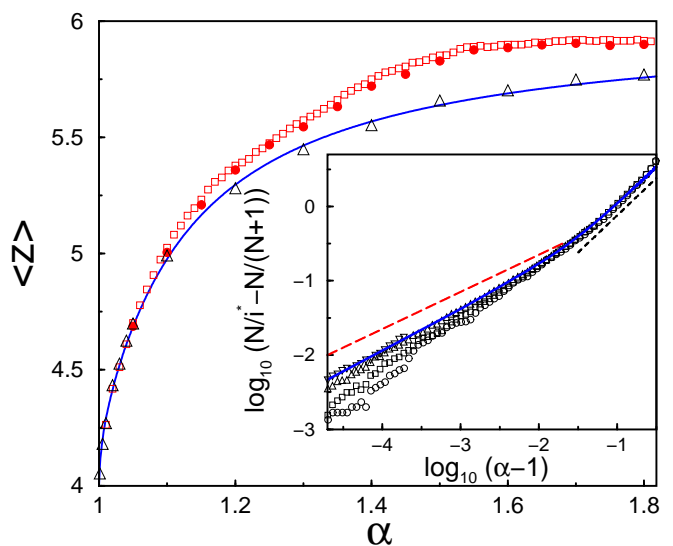


FIG. 4: (Color online) Contact number  $\langle z \rangle$  vs.  $\alpha$  for compression (triangles) and annealing ( $\Delta\alpha = 0.005$  (open squares) and 0.05 (filled circles)) packing-generation methods for  $N = 480$ .  $\langle z \rangle$  for the annealing method diverges from that for the compression method for  $\alpha > 1.1$ . The solid line follows  $\langle z \rangle = 6 - i^*(\alpha)/(3N)$  for the compression method data. The inset shows the system size dependence of  $N/i^*(\alpha) - N/(N+1)$  for  $N = 120$  (circles), 240 (squares), 960 (upward triangles), and 1920 (downward triangles). (Data at large  $N$  is limited to small  $\alpha$ .) The red (black) dashed line has slope 0.5 (1.0). The solid line is an interpolation between power-laws of 0.5 at small  $\alpha - 1$  and 1.0 at large  $\alpha - 1$ .

has significantly more structure than  $D(\omega)$  of disk packings for  $\omega > 10$ . These new features in  $D(\omega)$  will be investigated in more detail in future work [20]. Note that we have verified that all of the vibrational properties described here also hold for packings in which ellipses interact pairwise via the Gay-Berne potential [22] with a simpler form for the overlap function than that given in Eq. 2.

*Hypostaticity* Our analysis of the structural and mechanical properties of soft ellipse packings has led to several novel observations: (1) The quartic modes that exist for hard ellipse packings develop a quadratic contribution at finite overcompression, and therefore compression *stabilizes* static ellipse packings[8]; (2) The contribution of these quartic modes to the density of vibrational modes decreases as the aspect ratio increases; and (3) Static packings of ‘just touching’ ellipses are generically hypostatic, as shown in Fig. 4, with smaller average contact number  $\langle z \rangle$  than that predicted from isostatic counting arguments [21], i.e.  $\langle z \rangle_{\text{iso}} = 6$  for ellipses at any  $\alpha$ . Hypostatic packings have fewer contacts than required to satisfy all of the force and torque balance conditions, and thus in some directions of configuration space these packings are only quartically, not quadratically stable to perturbations. We find that the quartic modes represent collective, primarily rotational motions of the ellipses, which do not lead to cage breaking and particle rearrangements. Thus, we expect that if the isostatic counting argument is reformulated so that the quartic modes are not constrained, the average contact number measured in our simulations will match the minimum number of

contacts necessary to constrain the modes that are quadratically stable. In this sense, static ellipse packings are isostatic with respect to only the *quadratic* modes.

When each internal degree of freedom in a static ellipse packing is stabilized, the isostatic conjecture gives  $N\langle z \rangle/2 = 3N - 1$ . If it is not necessary to constrain the quartic modes, as conjectured above, this equation can be rewritten as

$$\frac{N\langle z \rangle}{2} = 3N - i^*(\alpha), \quad (4)$$

where  $N_4 = i^*(\alpha) - 1$  is the number of quartic modes in region (1) of the frequency spectrum. Thus, by measuring the number of quartic modes, we are able to determine  $\langle z \rangle(\alpha)$ . In the inset to Fig. 4, we show that  $N/i^*(\alpha) - N/(N+1)$  has two power-law regimes: scaling as  $\sqrt{\alpha-1}$  ( $\alpha-1$ ) for small (large)  $\alpha-1$ . In these limits, we obtain

$$\langle z \rangle(\alpha) = \langle z \rangle(1) + 2 \frac{A_n(\alpha-1)^n}{1 + A_n(\alpha-1)^n}, \quad (5)$$

where  $n = 0.5$  (1) in the small (large)  $\alpha-1$  limit and  $A_{0.5}$  and  $A_1$  are positive constants. In Fig. 4, we use a function that interpolates between these two power-laws and allows us to fit  $\langle z \rangle$  over the entire range of  $\alpha$ . These arguments imply that  $\langle z \rangle = \langle z \rangle_{\text{iso}}$  in the  $\alpha \rightarrow \infty$  limit, yet this is still an open question. We note that previous studies have predicted that the deviation  $\langle z \rangle(\alpha) - \langle z \rangle(1)$  should scale as  $\sqrt{\alpha-1}$  based on the behavior of the pair distribution function  $g(r)$  near contact for jammed systems composed of spherical particles [8]. In contrast, our numerical results show that the origin of hypostaticity in static ellipse packings can be determined from the number of quartic modes.

*Annealed packings* The static ellipse packings discussed up to this point were generated using a protocol in which ellipses at fixed aspect ratio are compressed to the just-touching state. Using this packing-generation method, we obtained a similar contact number versus aspect ratio curve to that obtained previously for jammed packings of hard ellipses. Since ellipse packings are hypostatic, it is in principle possible to obtain packings with higher  $\langle z \rangle$  than found in Fig. 4 without increasing the translational or orientational order. To test this, we developed an ‘annealing’ packing-generation method, which creates static packings by incrementally increasing the aspect ratio from  $\alpha = 1$ . The annealing method is the following. We initially create static bidisperse disk packings. Each disk is then assigned the same aspect ratio  $1 + \Delta\alpha$  with the direction of the long axis chosen randomly. A new static ellipse packing is formed from this initial state using the compression method described above. The ellipses of the new static packing are elongated again along their defined major axes, and the protocol is repeated until a static ellipse packing with the desired aspect ratio is reached.

Using this method, static ellipse packings can be generated that are denser and possess contact numbers much closer to  $z_{\text{iso}} = 6$  as shown in Fig. 4. The annealed packings still exhibit a low-frequency gap, and the location,  $i^*$ , of this gap can

be used to predict  $\langle z \rangle$  through Eq. 4. The variation of  $i^*$  with aspect ratio, however, differs from the ‘compressed’ packings. The annealed packings tend to have higher  $\langle z \rangle$  and fewer quartic modes. We found little variation of  $\langle z \rangle$  with changes in the increment  $\Delta\alpha$ . In future studies, we will employ molecular dynamics simulations to create just-touching static ellipse packings as a function of thermal quenching and compression rates to understand what variables strongly affect the number of quartic modes and thus control the contact number in systems composed of anisotropic particles.

Support from NSF grant nos. DMR-0549762 (BC & MM), DMR-0448838 (CSO) and CDI-0835742 (CS) is acknowledged. We acknowledge helpful conversations with Max Bi, Gregg Lois, Tom Witten, Ning Xu, and Zorana Zeravcic.

- 
- [1] A. J. Liu and S. R. Nagel, *Nature* **396**, 21 (1998).
  - [2] C. S. O’Hern, L. E. Silbert, A. J. Liu, and S. R. Nagel, *Phys. Rev. E* **68**, 011306 (2003).
  - [3] H. A. Makse, D. L. Johnson, and L. M. Schwartz, *Phys. Rev. Lett.* **84**, 4160 (2000).
  - [4] C. S. O’Hern, S. A. Langer, A. J. Liu, and S. R. Nagel, *Phys. Rev. Lett.* **88**, 075507 (2002).
  - [5] M. Wyart, S. R. Nagel, and T. A. Witten, *Europhys. Lett.* **72**, 486 (2005).
  - [6] M. Wyart, L. E. Silbert, S. R. Nagel, and T. A. Witten, *Phys. Rev. E* **72**, 051306 (2005).
  - [7] E. Somfai, M. Van Hecke, W. G. Ellenbroek, K. Shundyak, and W. Van Saarloos, *Phys. Rev. E* **75**, 020301(R) (2007).
  - [8] A. Donev, R. Connelly, F. H. Stillinger, and S. Torquato, *Phys. Rev. E* **75**, 051304 (2007).
  - [9] A. Donev, I. Cisse, D. Sachs, E. A. Variano, F. H. Stillinger, R. Connelly, and S. Torquato, *Science* **303**, 990 (2004).
  - [10] G.-J. Gao, J. Bławdziewicz, and C. S. O’Hern, *Phys. Rev. E* **74**, 061304 (2006).
  - [11] H. P. Zhang and H. A. Makse, *Phys. Rev. E* **72**, 011301 (2005).
  - [12] J.W. Perram and M.S. Wertheim, *J. Comp. Phys.* **58**, 409 (1985).
  - [13] J.W. Perram, J. Rasmussen, E. Praestgaard, J.L. Lebowitz, *Phys. Rev. E* **54**, 6565 (1996).
  - [14] B. J. Berne and P. Pechukas, *J. Chem. Phys.* **46**, 4213 (1972).
  - [15] D. J. Cleaver, C. M. Care, M. P. Allen, and M. P. Neal, *Phys. Rev. E* **54**, 559 (1996).
  - [16] The parameters  $\sigma_0$ ,  $\beta$ , and  $\chi$  in Eq. 2 are defined as  $\sigma_0 = \sqrt{\frac{b_j^2}{\lambda} + \frac{b_j^2}{1-\lambda}}$ ,  $\beta = \left( \frac{(a_j^2 - b_j^2)(a_j^2 + \frac{1-\lambda}{\lambda} b_j^2)}{(a_j^2 - b_j^2)(a_j^2 + \frac{\lambda}{1-\lambda} b_j^2)} \right)^{1/4}$ , and  $\chi = \left( \frac{(a_j^2 - b_j^2)(a_j^2 - b_j^2)}{(a_j^2 + \frac{1-\lambda}{\lambda} b_j^2)(a_j^2 + \frac{\lambda}{1-\lambda} b_j^2)} \right)^{1/2}$ .
  - [17] J. A. Cuesta and D. Frenkel, *Phys. Rev. A* **42**, 2126 (1990).
  - [18] A. Tanguy, J. P. Wittmer, F. Leonforte, and J.-L. Barrat, *Phys. Rev. B* **66**, 174205 (2002).
  - [19] In the following discussion, we have accounted for rattler ellipses and set  $N = N'$ .
  - [20] M. Mailman, C. Schreck, B. Chakraborty, and C. S. O’Hern (unpublished).
  - [21] A. V. Tkachenko and T. A. Witten, *Phys. Rev. E* **60**, 687 (1999).
  - [22] J. G. Gay and B. J. Berne, *J. Chem. Phys.* **74**, 3316 (1981).